ARTICLE NO. 79-4114

# Active External Store Flutter Suppression in the YF-17 Flutter Model

E. Nissim* and I. Lottati†
*Technion – Israel Institute of Technology, Haifa, Israel*

**A single activated trailing-edge (T.E.) control system (spanning 7% of each wing) is applied to the YF-17 flutter model with the object of suppressing the external store flutter of three different store configurations. The control law is derived by the use of the aerodynamic energy concept and its gains are maintained constant for all three configurations. The results obtained show that the activated T.E. control system leads to very significant increases in the flutter dynamic pressures ($Q_{DF}$) of all three configurations; these increases range between 160-240% increase in $Q_{DF}$. These increases in $Q_{DF}$ are maintained over a very wide range of flight altitudes and flight velocities.**

## Nomenclature

$a_1, a_2$ = coefficients defined in Eq. (2)
$b$ = semichord length at control surface midspan section
$g$ = structural damping
$i$ = $\sqrt{-1}$
$h_l$ = displacement of 30% chord point at control surface midspan section
$h_r$ = displacement of the fuselage reference point
$M$ = Mach number
$Q_D$ = flight dynamic pressure
$Q_{DF}$ = flutter dynamic pressure
$Q_{D\,\min.}$ = the minimum value of $Q_D$ of the three open-loop wing/store configuration
$Q_{D\,\max.}$ = $2 \cdot Q_{D\,\min.}$
$R_T$ = filter transfer function defined in Eq. (1)
$S$ = $i\omega$
$V$ = flight velocity
$\alpha_l$ = angle of attack at control surface midspan section
$\alpha_r$ = angle of attack at the fuselage reference point
$\delta$ = deflection of the trailing-edge control surface, positive downward
$\omega$ = frequency of oscillation
$\omega_{n1}, \omega_{n2}$ = natural frequencies of filter [see Eq. (2)]
$\zeta_1, \zeta_2$ = damping coefficients [see Eq. (2)]
$(\ \dot{}\ )$ = differentiation with respect to time

## Introduction

THE technological advances made in recent years in the field of control systems and the increased reliability of control system components have stimulated considerable interest in the possibilities of suppressing flutter by means of active controls. A considerable number of analytical and experimental works[1-14] have recently been published showing the possibility and advantages of using active flutter suppression systems. However, a problem common to all flutter suppression control systems is a tendency to be very sensitive to changing flight conditions and to vehicle configuration.[1,15] This sensitivity implies that a control system designed to suppress flutter for a specified vehicle configuration and a specified flight condition, may show a degraded performance or even show detrimental effects at other flight conditions or at different configurations. The aerodynamic energy concept was developed[16] with the object of deriving control laws which are both effective in suppressing flutter and are also insensitive to system changes (that is to changes in flight conditions or to changes in vehicle configuration). The results included in the original derivation of the aerodynamic energy concept[16] have demonstrated the ability of the combined activated leading-edge (L.E.) = trailing-edge (T.E.) control system to achieve the objectives of both flutter suppression and insensitivity to system changes. This insensitivity to system changes was achieved in Ref. 16 by imposing a sufficient but not a necessary condition for stability. The T.E.-alone control system however was shown[16] to be inferior to the L.E.-T.E. control system (within the limits of the preceding assumptions), and its ability to achieve the aforementioned objectives was doubtful. Application of the general results of Ref. 16 to specific aircraft[17] had demonstrated the effectiveness of the L.E.-T.E. control system in the simultaneous solution of both flutter suppression and gust alleviation problems. There has been considerable reluctance however to accept an activated L.E. control system due to the large hinge moment required to control its motion and due to its possible detrimental effects on the general aerodynamic characteristics of the wing. T.E.-tab control systems have therefore been suggested[18] and shown to yield results similar to those of the L.E.-T.E. control system. Recent developments in the aerodynamic energy approach[19] have shown that by abandoning the sufficiency condition for stability, a relaxed condition can be formulated which insures the insensitivity of the control system to the changing flight conditions. The results of Ref. 19 show that a T.E.-only control system may meet the requirements of both stability and insensitivity to flight conditions. Application of the foregoing new developments to a specific problem of a drone aircraft[20] has demonstrated the ability of the T.E. control system to act on its own as a flutter suppressor. A comparison has recently been made[21] between the performance of a T.E.-alone control system and the performance of a L.E.-T.E. control system when applied to a specific flutter example of a drone aircraft. The results of this comparison demonstrate that the performance of the T.E.-alone control system can be made comparable to (or even exceed) the performance of the L.E.-T.E. control system treated in Ref. 21. In Ref. 22 a com-

Received Jan. 9, 1978; revision received Sept. 8, 1978. 

Index categories: Aeroelasticity and Hydroelasticity; Guidance and Control.

*Professor, Dept. of Aeronautical Engineering. Member AIAA.
†Aeronautical Engineer, Dept. of Aeronautical Engineering.

parison is made between the performance of a T.E. control system as designed by the application of the relaxed energy approach[19,20] and the performance of a similar control system, as designed by classical control theory. This comparison demonstrates both the effectiveness and the superiority of the control system designed by the relaxed aerodynamic energy concept.

All of the examples just described[17,20-22] included a fairly wide range of variation of flight conditions. This variation included changes in both flight altitude and in the flight Mach number. However, none of the examples included any changes in the aircraft configuration. Changes made in aircraft configuration can clearly serve as a more severe test to the insensitivity of a control system to system changes. It is therefore the purpose of the present work to apply an activated T.E.-alone control system to a problem of external store flutter, where three distinctly different store configurations yield low flutter speeds, and to demonstrate the ability of the activated system to suppress all three flutter speeds using a single control law with constant gains.

## Description of External Store Flutter Example

### System Description

The external store flutter example treated in this work consists of the YF-17 flutter model. Figure 1 shows the plan view of one wing and half of the horizontal tail of the model. There are three control surfaces on each wing: one L.E. control surface and two T.E. control surfaces. Only the outboard T.E. control surface will be activated in the present work. The choice of this outboard control surface follows the

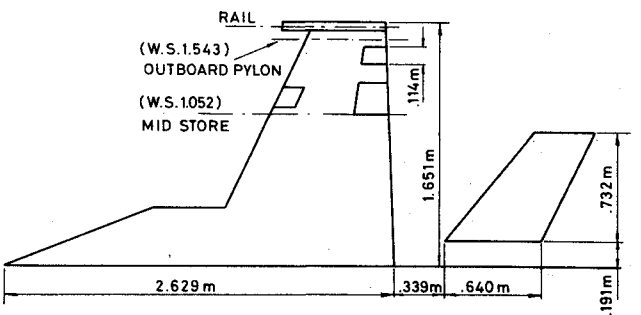


**Fig. 1 Plane view (schematic) of YF-17 flutter model.**

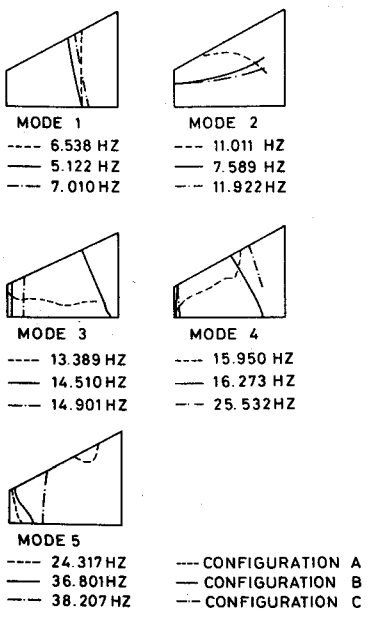


**Fig. 2 Node lines—YF-17 flutter model, configurations A,B, and C.**

**Table 1 Description of the three configurations**

| Description | Configuration A | B | C |
|---|---|---|---|
| Tip launcher rail | AIM-9E (flexible) | Empty | Empty |
| W.S.1.543 pylon | Not installed | AIM-7S(rigid) | AIM-9E(rigid) |
| W.S.1.052 pylon | AIM-7 (rigid) | Not installed | Not installed |
| $\omega_{n1}$ [a] | 6.5377 | 5.1218 | 7.0099 |
| $\omega_{n2}$ | 11.0111 | 7.5891 | 11.9223 |
| $\omega_{n3}$ | 13.3887 | 14.5104 | 14.9007 |
| $\omega_{n4}$ | 15.9500 | 16.2730 | 25.5323 |
| $\omega_{n5}$ | 24.3176 | 36.8006 | 38.2069 |
| $\omega_{n6}$ | 38.2780 | 38.5456 | 41.3348 |
| $\omega_{n7}$ | 44.4797 | 43.0960 | 46.9919 |

[a] $\omega_{n,i}$ = natural frequency of the $i$th elastic mode in Hz.

results of Ref. 17, where it had been shown that for flutter suppression purposes, the optimum location of the control surface should be as near the tip of the wing as is structurally possible. The span of this outboard control surface is around 7% of the semispan of the wing. This value of control surface span is smaller than those employed in previous works[17,20,21] (that is, 10-12% of wing semispan) and may therefore affect the values associated with the control surface activity. However, it was felt that for the purpose of the present work no modifications need be introduced in the existing flutter model, and therefore no resizing or relocation of this existing control surface will be attempted. Table 1 describes the external stores which constitute each of the three configurations treated herein together with the natural frequencies associated with the first seven symmetric elastic modes for each configuration (see also Fig. 1). The plan view of the wing describing the first five elastic modes for each configuration are shown in Fig. 2. The horizontal tail surface is assumed rigid.

### Control Law

The general form of the control law employed in this work was established in Ref. 19 using the relaxed energy approach. The control law for the T.E. control surface is given by the following general form:

$$\delta = -1.86(\alpha_l - \alpha_r) + R_T \lfloor 4 \quad 2.8 \rfloor \begin{Bmatrix} \dfrac{h_l - h_r}{b} \\ \alpha_l - \alpha_r \end{Bmatrix} \tag{1}$$

where $\delta$ is the deflection of the T.E. control surface (Fig. 3) and where $h_l$, $\alpha_l$ denote the translation and rotation of the 30% chord point at the control surface midspan section, respectively (see Fig. 3). The parameters $h_r$ and $\alpha_r$ similarly denote the translation and rotation of a reference point located along the centerline of the fuselage, and $b$ denotes the semichord length at the control surface midspan section (see Fig. 3). $R_T$ is defined by the following expression (see also Refs. 19 and 20):

$$R_T = \frac{a_1 S^2}{S^2 + 2\zeta_1 \omega_{n1} S + \omega_{n1}^2} + \frac{a_2 S^2}{S^2 + 2\zeta_2 \omega_{n2} S + \omega_{n2}^2} \tag{2}$$

where $S = i\omega$ and where $\omega$ represents frequency of oscillation. The parameters $a_i$, $\zeta_i$, $\omega_{ni}$ are all positive and their values determined by an optimization program based on the gust response of the aircraft under consideration, following the method of Ref. 20.

### Mathematical Model

The equations of motion were formulated and solved in an identical manner as in Refs. 20 and 22. The equations of

motion included, for each configuration two rigid-body modes (plunge and pitch) plus seven symmetric elastic modes. The generalized aerodynamic forces were computed using the Doublet-Lattice method with 126 boxes on each wing and 32 boxes on each half-horizontal tail surface.

**Flutter Suppression Objectives**

In the absence of a definition of the desired flight envelope for the flutter model, the following objectives were arbitrarily set for achievement by the activated YF-17 flutter model (maintaining the Mach number $M=0$ throughout the present investigation):

1) The model should be able to fly with a value of dynamic pressure $Q_D$ which is twice the value of the minimum flutter dynamic pressure ($Q_{D\,\min.}$) of the unactivated model. Since there are three external store configurations, $Q_{D\,\min.}$ refers therefore to the configuration which yields the minimum flutter dynamic pressure.

2) Flutter suppression should be achieved with a minimum value for control surface rates.

3) The stability of all three external store configurations should be maintained for all values of $Q_D \leq 2Q_{D\,\min.}$ using fixed control gains and with no substantial degradation in the control surface rates (to be referred to as control surface activity).

## Presentation and Discussion of Results

It has been shown in Refs. 20 and 22 that for any chosen control law the equations of motion are essentially a function of $Q_D$ and $M$ only. However, for the case of $M=0$, the equations of motion will be a function of $Q_D$ and of the flight velocity $V$. Therefore, for any fixed value of $V$ at $M=0$, a variation in $Q_D$ is equivalent to a variation in altitude. The flutter results will be presented for any fixed value of $V$ by a root locus type of plot with $Q_D$ acting as a parameter. Its variation in the present work will be made to span the range of $0 \leq Q_D \leq 9.58$ KPa (1 KPa = 1000 N/m$^2$). In the following, the open-loop flutter characteristics relating to the three different external store configurations will first be presented. A control law is then derived and its effects on the flutter speeds of the preceding three configurations is then tested and discussed.

The effectiveness of the activated T.E. control system can only be assessed by comparison with the open-loop system. The open-loop root locus plots for configurations A,B,C with $V=98$ m/s and zero structural damping, $g=0$, are presented in Figs. 4-6 as examples of the open-loop behavior of the flutter model considered herein as a function of dynamic pressure. It can be seen that configuration B is the most critical from the point of view of flutter, yielding the lowest value of $Q_D$ at flutter, i.e., $Q_{D\,\min.} = 2.63$ KPa. Configuration A can be seen to be less critical, yielding a value of $Q_{DF} = 3.64$ KPa, whereas configuration C appears to be the least critical yielding the value of $Q_{DF} = 4.31$ KPa. The values of $Q_{DF}$ relating to flight speeds of $V=120$ m/s and $V=145$ m/s are presented in the summary in Table 2 for the three configurations. As can be seen, the values of $Q_{DF}$ for each configuration remain essentially unchanged. The objective of the present work will therefore be to determine a control law with fixed gains, which will enable the flutter model to fly at a dynamic pressure $Q_D = 5.26$ KPa (to be referred to as $Q_{D\,\max.}$) without encountering flutter and with minimum control activity. This case is interesting since all three configurations yield flutter speeds which correspond to $Q_D < 5.26$ KPa. Hence, the activated control system should be effective for all configurations in order to achieve the objectives of the present work.

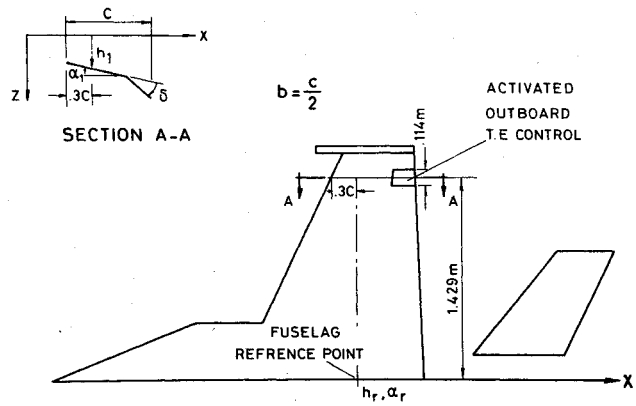


**Fig. 3 Geometrical description of the active control system.**

## Determination of the Control Law Parameters

The control law parameters are determined through the use of an optimization program which minimizes the root-mean-square (rms) deflection rates of the control surface due to a unit rms gust input based on the Von Karman gust spectrum. This procedure is described in detail in Ref. 20.

**Table 2 Summary of results**

| | Open-loop flutter | | | Closed-loop – activated outboard T.E. control surface | | | | | | | | |
|---|---|---|---|---|---|---|---|---|---|---|---|---|
| | $g=0$ | | | $g=0$ | | | $g=0.015$ | | | $g=0.03$ | | |
| Configuration | A | B | C | A | B | C | A | B | C | A | B | C |
| Flutter $Q_D$, KPa | | | | | | | | | | | | |
| $V=98$ m/s | 3.64 | 2.63 | 4.31 | 8.91 | 8.95<br>8.95<br>7.80 | 8.52 | ... | ... | ... | ... | ... | ... |
| $V=120$ m/s | 3.54 | 2.68 | 4.26 | 8.67 | 8.76<br>6.66 | 8.38 | ... | ... | ... | ... | ... | ... |
| $V=143$ m/s | 3.50 | 2.73 | 4.26 | 8.62 | 8.67 | 8.33 | ... | ... | ... | ... | ... | ... |
| Max. value of $\dot{\delta}_{rms}$, deg/s/m/s | | | | | | | | | | | | |
| $V=98$ m/s | ... | ... | ... | 83 | 161 | 156 | 72 | 87 | 121 | 65 | 68 | 104 |
| $V=120$ m/s | ... | ... | ... | ... | ... | ... | 65 | 74 | 114 | ... | ... | ... |
| $V=143$ m/s | ... | ... | ... | ... | ... | ... | 59 | 75 | 108 | ... | ... | ... |
| Max. value of $\delta_{rms}$, deg/m/s | | | | | | | | | | | | |
| $V=98$ m/s | ... | ... | ... | 2.39 | 4.17 | 3.15 | 2.23 | 2.53 | 2.69 | 2.10 | 2.17 | 2.49 |
| $V=120$ m/s | ... | ... | ... | ... | ... | ... | 1.97 | 2.30 | 2.46 | ... | ... | ... |
| $V=143$ m/s | ... | ... | ... | ... | ... | ... | 1.77 | 2.13 | 2.26 | ... | ... | ... |

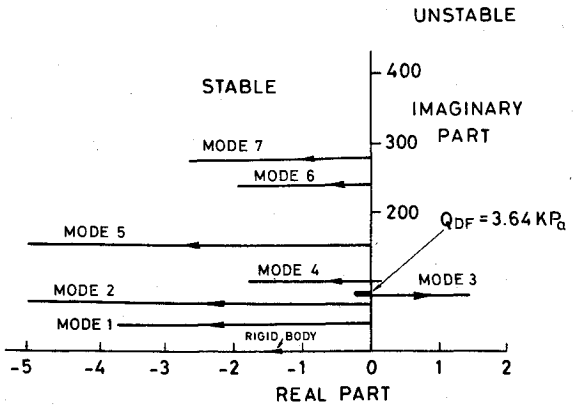


**Fig. 4 Root locus plot – open loop, configuration A (with $V = 98$ m/s).**

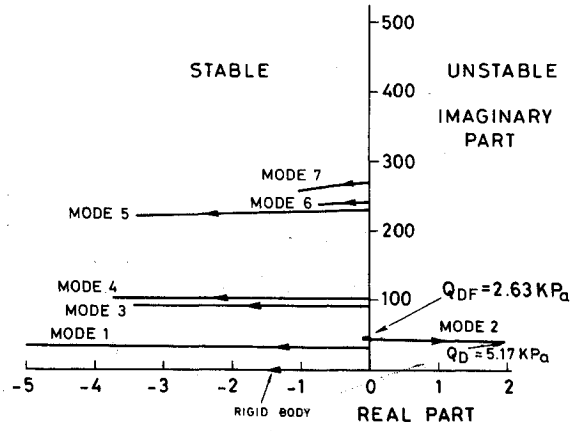


**Fig. 5 Root locus plot – open loop, configuration B (with $V = 98$ m/s).**

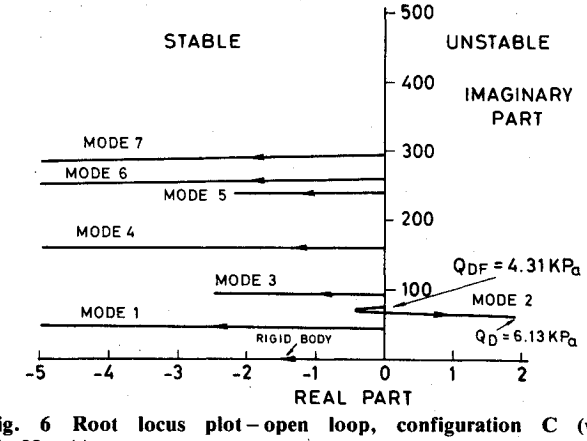


**Fig. 6 Root locus plot – open loop, configuration C (with $V = 98$ m/s).**

For the purpose of the present example, configuration B was chosen for the determination of the control law gains. This choice of configuration B follows the preceding open-loop results which indicate its being the most critical configuration for flutter. The optimization was performed for $Q_D = 5.26$ KPa, $V = 98$ m/s, structural damping $g = 0$, and with the following constraints on the optimization parameters (see Ref. 20 for further details):

$$0 \le a_i \le 4.5 \tag{3a}$$

$$0.5 \le \zeta_i \le 1. \tag{3b}$$

$$30. \le \omega_{ni} \le 70. \text{rad/s} \tag{3c}$$

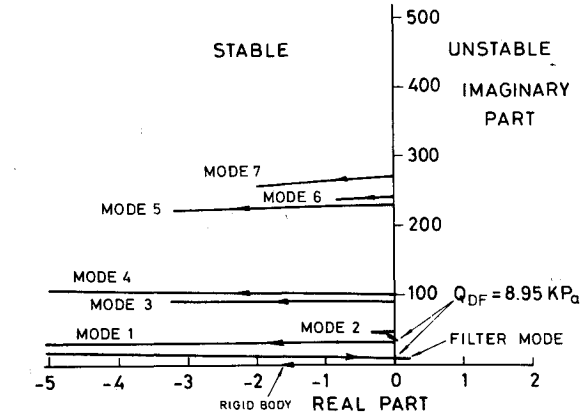


**Fig. 7 Root locus plot – closed loop, configuration B (with $V = 98$ m/s).**

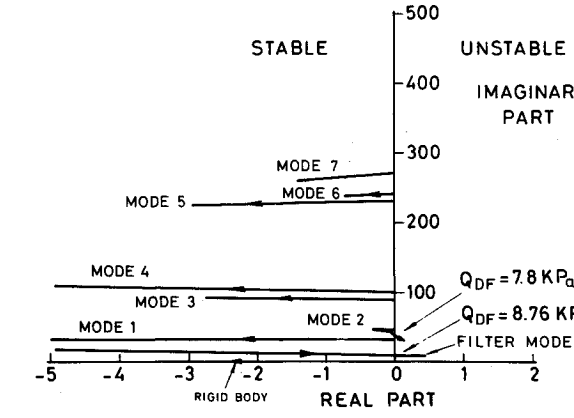


**Fig. 8 Root locus plot – closed loop, configuration B (with $V = 120$ m/s).**

The optimization procedure yields the following optimal control law:

$$\delta = \left[ \lfloor 0 \quad -1.86 \rfloor + \frac{4.5\,S^2}{S^2 + 2 \times 0.5 \times 30S + (30)^2} \lfloor 4 \quad 2.8 \rfloor \right] \times \begin{Bmatrix} \dfrac{h_l - h_r}{b} \\ \alpha_l - \alpha_r \end{Bmatrix} \tag{4}$$

with

$$\dot{\delta}_{\text{rms}} = 161 \text{ deg/s/m/s}$$

$$\delta_{\text{rms}} = 4.17 \text{ deg/m/s}$$

The meaning of the different parameters of the control law [Eq. (4)] is explained in both Refs. 19 and 20. There is no intention to repeat the various details herein except for the statement that the preceding results show that for minimum control rates, maximum damping is introduced around the frequencies of 30 rad/s whereas the flutter frequency is around 44 rad/s. The distribution with frequency of the introduced damping is fairly wide as implied by $\zeta = 0.5$. The control deflection introduces positive aerodynamic stiffness terms at frequencies larger than 30 rad/s and negative aerodynamic stiffness terms at frequencies lower than 30 rad/s. It is also interesting to note that all the optimized values of the control surface parameters are on the optimization constraints defined by Eq. (3).

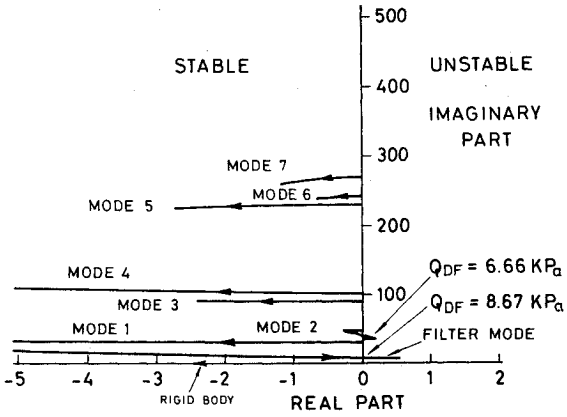


Fig. 9 Root locus plot – closed loop, configuration B (with $V = 143$ m/s).

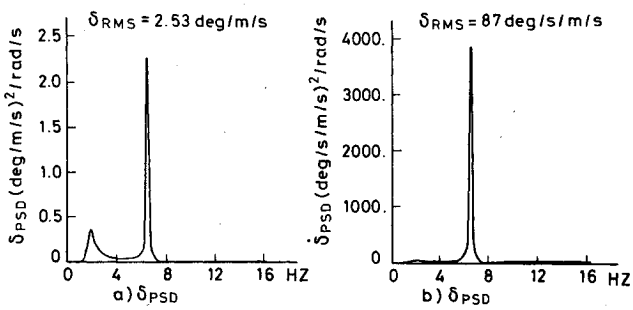


Fig. 10 PSD of control surface response – configuration B (with $V = 98$ m/s, $g = 0.015$, and $Q_D = 5.26$ KPa).

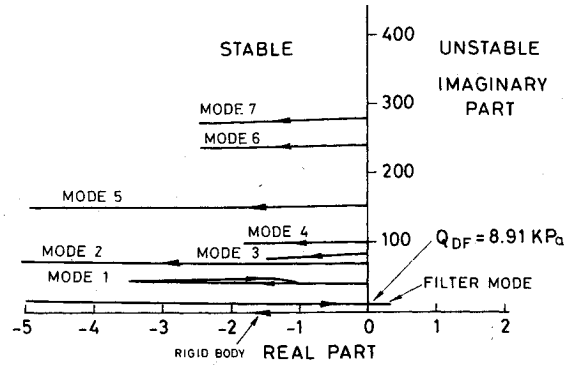


Fig. 11 Root locus plot – closed loop, configuration A (with $V = 98$ m/s).

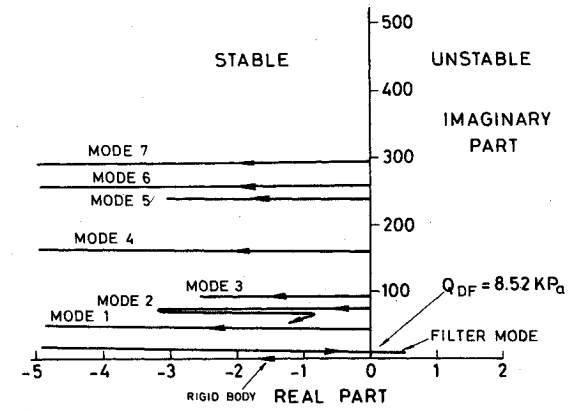


Fig. 12 Root locus plot – closed loop, configuration C (with $V = 98$ m/s).

## Performance of the Closed-Loop Control System

The performance of the closed-loop control system will be presented for each of the three configurations considered herein. A short discussion relating to all three configurations will then be presented. Since the optimization procedure[20] was applied to configuration B, its closed-loop performance will first be presented.

### Results for Configuration B

Figures 7-9 represent the closed-loop root locus plots for $V = 98$ m/s, $V = 120$ m/s, and $V = 143$ m/s, respectively. Each of the root locus plots yields two flutter dynamic pressures. One flutter dynamic pressure around $Q_{DF} = 8.7$ PKa comes about due to the active filter mode. The second flutter dynamic pressure varies within the range $6.66 \leq Q_{DF} \leq 8.95$ KPa and it originates from the structural modes. As can be seen in the figures, the closed-loop flutter branch due to the structural modes yields an extremely mild instability. Therefore, small changes in damping yield relatively large changes in the flutter dynamic pressure. However, only a very small amount of structural damping will be necessary to turn this flutter branch stable (for stability up to the maximum value of $Q_D$ used in this work, i.e. $Q_D = 9.58$ PKa and $V = 143$ m/s, a value of $g = 0.0035$ will be necessary; see Fig. 9) and its existence is therefore of academic nature. It can therefore be concluded that the optimized closed-loop flutter dynamic pressure is much higher than $Q_{D\,\max.}$ ($= 5.26$ KPa).

An example of the PSD distribution for control deflection and control rate deflection is shown in Fig. 10 which relates to the case where $Q_D = 5.26$ KPa, $g = 0.015$, and $V = 98$ m/s. As can be seen the peak deflection rate of the control surface is around the open-loop flutter frequency. The control surface deflection shows a second peak around 12 rad/s which relates to a filter mode. The rms control rate assumes the value of 87 deg/s/m/s, whereas the rms control deflection assumes the value of 2.53 deg/m/s. The results pertaining to $V = 120$ m/s and $V = 143$ m/s, while maintaining $Q_D = 5.26$ KPa, are presented in Table 2 together with the results relative to $V = 98$ m/s, $g = 0$, and $g = 0.03$. It can be seen from Table 2 that the control surface activity reduces with increase in the values of the structural damping $g$ and with the increase in flight velocity $V$.

### Results for Configurations A and C

Figures 11 and 12 represent the closed-loop root locus plots for configurations A and C, respectively, with $V = 98$ m/s, and $g = 0$. In both configurations the open-loop structural mode flutter branch has been completely suppressed. The mode which turns unstable at around $Q_D = 8.5$-$8.9$KPa is a filter mode which originates from the introduction of a control surface degree of freedom. Similar results are obtained when changing $V$ to assume the values of $V = 120$ m/s and $V = 143$ m/s. The results are summarized in Table 2 and they indicate that the flutter dynamic pressure for the preceding two configurations remains within the range of $8.33 \leq Q_{DF} \leq 8.91$ KPa. These values for $Q_{DF}$ are much larger than both the corresponding open-loop flutter dynamic pressures and the value of $Q_{D\,\max.}$. Hence the control law defined by Eq. (4) leads to a very large increase in the value of $Q_{DF}$ for all three configurations considered in this work.

Figures 13 and 14 show the PSD distributions for both the control surface deflection rates and the control surface deflections for both configurations with $Q_D = 5.26$ KPa, $V = 98$ m/s, and $g = 0.015$. Here again the peak deflection rates lie around the corresponding open-loop flutter frequencies whereas the peak deflections show a second peak corresponding to the filter frequency. The rms control surface activities over a range of values of $g$ (that is $g = 0$, $g = 0.015$,

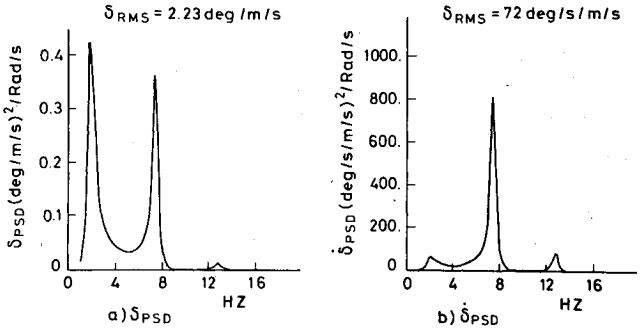


**Fig. 13 PSD of control surface response – configuration A (with $V = 98$ m/s, $g = 0.015$, and $Q_D = 5.26$ KPa).**

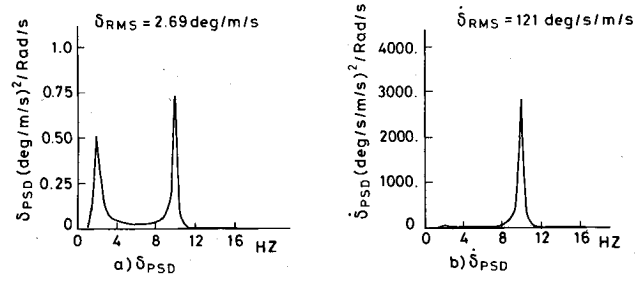


**Fig. 14 PSD of control surface response – configuration C (with $V = 98$ m/s, $g = 0.015$, and $Q_D = 5.26$ KPa).**

and $g = 0.03$) and a range of values of $V$ (that is $V = 98$ m/s, $V = 120$ m/s, and $V = 143$ m/s) are summarized in Table 2. As can be noted, the most demanding requirement for the control surface deflection rates originates from configuration C which has the highest open-loop value for $Q_{DF}$.

## General Discussion of Results

It should be stressed again at this stage that the single control law defined by Eq. (4), which has fixed gains, leads to very large increases in the flutter dynamic pressures of all three configurations treated in this work. The closed-loop values of $Q_{DF}$ are much larger than the value of $Q_{D\,\max.}$ (= 5.26 KPa), which was presented as an objective for the present work. It appears surprising however that the least critical configuration (that is configuration C) from the flutter point of view turns out to be the most demanding in terms of control surface activity. Sensitivity tests indicate the potential of the parameter $a_1$ [ = 4.5 in Eq. (4)] in reducing the overall activity of the control system. Figure 15 shows such a sensitivity sweep of the parameter $a_1$ (for $Q_D = 5.26$ KPa, $V = 98$ m/s, and $g = 0.015$) and it indicates that by reducing $a_1$, some reductions in control activity may be obtained. However, this line was not further pursued in this investigation since general trends and results form the main objectives of the present work rather than refined results which follow a series of repeated analyses directed toward a finalized design. In this latter case one cannot ignore such important parameters as control surface span and control surface location. As already stated earlier in this work, the span of the control surface treated in this work is relatively small. The increase in control surface span may lead to a very significant reduction in control surface activity for all configurations. Figure 16 shows the results of another sensitivity test as applied to the variation of the dynamic pressure $Q_D$ (with $V = 98$ m/s and $g = 0.015$). As already stated, a reduction in $Q_D$ while keeping $V$ constant is equivalent to increasing the flight altitude. As can be seen from Fig. 16 the lowest flight altitude presents the most critical condition for control surface activity. Other parameter variations were conducted and the results indicated that the control law defined by Eq. (4) has no problems associated with parameter sensitivities.

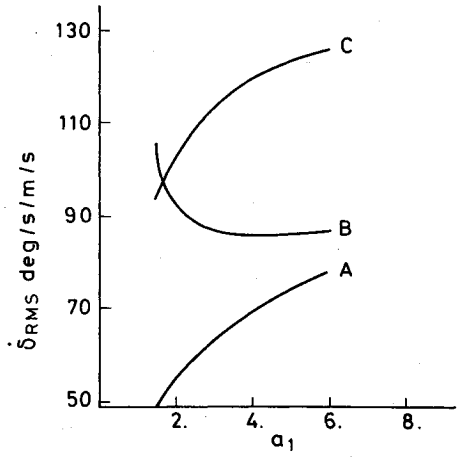


**Fig. 15 Variation with $a_1$ of rms response of control surface (with $V = 98$ m/s, $g = 0.015$, and $Q_D = 5.26$ KPa).**

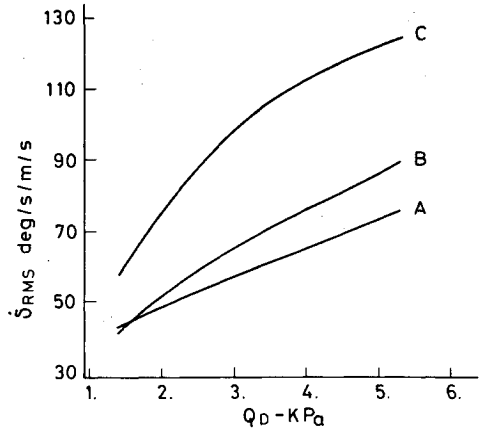


**Fig. 16 Variation with $Q_D$ of rms response of control surface (with $V = 98$ m/s, $g = 0.015$, and $Q_D = 5.26$ KPa).**

## Conclusions

The ability of the activated T.E. control surface to successfully cope with three different external store flutter configurations over a range of flight speeds and flight altitudes has been demonstrated. The significance of the results obtained in this work are threefold:

1) A single control law with fixed gains was employed for all configurations.

2) Very large increases in the flutter dynamic pressures were obtained for all configurations.

3) The effectiveness of the activated T.E. control system over the whole range of flight conditions and flight configurations provides yet another confirmation regarding the potential power of the relaxed aerodynamic energy concept.

## Acknowledgments

This work is a part of a study supported by NASA under Grant NSG-7072.

## References

[1] Wykes, J.H. and Mori, S., "Techniques and Results of an Analytical Investigation into Controlling the Structure Modes of Flexible Aircraft," *AIAA Symposium on Structural Dynamics and Aeroelasticity*, Aug.-Sept. 1965, pp. 419-433.

[2] Wykes, J.H. and Mori, S., "An Analysis of Flexible Aircraft Structural Mode Control," Air Force Flight Dynamics Laboratory, Wright Patterson Air Force Base, Ohio, AFFDL-TR-65-T90, Pt. I, June 1966.

[3] Dempster, J.B. and Roger, K.L., "Evaluation of B-52 Structural Response to Random Turbulence with Stability Augmentation Systems," *Journal of Aircraft,* Vol. 4, Nov.-Dec. 1967, pp. 507-512.

[4] Rohling, W.J., "Flying Qualities, an Integral Part of a Stability Augmentation System," *Journal of Aircraft,* Vol. 6, Nov.-Dec. 1969, pp. 510-515.

[5] Dempster, J.B. and Arnold, J.I., "Flight Test Evaluation of Advanced Stability Augmentation System for the B-52 Aircraft," AIAA Paper 68-1068, Oct. 1968.

[6] Thompson, G.O. and Kass, G.J., "Active Flutter Suppression – An Emergency Technology," *Journal of Aircraft,* Vol. 9, March 1972, pp. 230-235.

[7] Topp. L.J., "Potential Performance Gains by Use of a Flutter Suppression System," Paper 7-B3, 1971, Joint Automatic Control Conference, St. Louis, Mo., Aug. 1971.

[8] Kordes, E.E., "Influence of Structural Dynamics on Vehicle Design – Government View," AIAA Paper 77-438, March 1977.

[9] Redd, L.T., Gilman, J., Jr., Cooley, D.E., and Sevart, F.D., "Wind-Tunnel Investigation of a B-52 Flutter Suppression System," *Journal of Aircraft,* Vol. 11, Nov. 1974, pp. 659-663.

[10] Sandford, M.C., Abel, I., and Gray, D.L., "Transonic Study of Active Flutter Suppression Based on Energy Concept," *Journal of Aircraft,* Vol. 12, Feb. 1975, pp. 72-77.

[11] Sanford, M.C., Abel, I., and Gray, D.L., "Development and Demonstration of a Flutter-Suppression System Using Active Controls," NASA TR R-450, 1975.

[12] Thompson, G.O. and Sevart, F.D., "Wind-Tunnel Investigation of Control Configured Vehicle Systems. Flutter Suppression and Structural Load Alleviation," AGARD-CP-175, April 1975, pp. 4.1-4.8.

[13] Swach, E. and Stearman, O., "Suppression of Flutter on Interfering Lifting Surfaces by the Use of Active Controls," AIAA Paper 74-404, April 1974.

[14] Roger, K.L., Hodges, G.E., and Felt, L., "Active Flutter Suppression – a Flight Test Demonstration," AIAA Paper 74-402, April 1974.

[15] Edwards, J.W., Breakwell, J.V., and Bryson, A.E., Jr., "Active Flutter Control Using Generalized Unsteady Aerodynamic Theory," AIAA Paper 77-1061, Aug. 1977.

[16] Nissim, E., "Flutter Suppression Using Active Controls Based on the Concept of Aerodynamic Energy," NASA TN D-6199, 1971.

[17] Nissim, E., Caspi, A., and Lottati, I., "Application of the Aerodynamic Energy Concept to Flutter Suppression and Gust Alleviation by Use of Active Controls," NASA TN D-8212, 1976.

[18] Nissim, E., "Active Flutter Suppression Using Trailing-Edge and Tab Control Surfaces," *AIAA Journal,* Vol. 14, June 1976, pp. 757-762.

[19] Nissim, E., "Recent Advances in Aerodynamic Energy Concept for Flutter Suppression and Gust Alleviation Using Active Controls," NASA TN D-8519, 1977.

[20] Nissim, E. and Abel, I., "Development and Application of an Optimization Procedure for Flutter Suppression Using the Aerodynamic Energy Concept," NASA TP 1137, Feb. 1978.

[21] Nissim, E., "Comparative Study Between Leading-Edge-Trailing-Edge and Trailing-Edge-Alone Active Flutter Suppression Systems," *Journal of Aircraft,* Vol. 15, Dec. 1978, pp. 843-848.

[22] Abel, I., Perry, B., and Murrow, H.N., "Synthesis of Active Controls for Flutter Suppression on a Flight Research Wing," AIAA Paper 77-1062, Aug. 1977.